JOURNAL OF MATERIALS SCIENCE **28** (1993) 5113–5122

Laser cladding of Mg–Al alloys

A. A. WANG, S. SIRCAR, J. MAZUMDER
Laser-Aided Materials Processing Laboratory, Department of Mechanical and Industrial Engineering, University of Illinois at Urbana-Champaign, 1206 West Green Street, Urbana, IL 61801, USA

Among rapid solidification processing methods, laser cladding is a unique and promising technique which can be used to increase the corrosion resistance of materials. This paper describes the improvement of the laser-cladding process for magnesium-based alloys and an investigation of the effect of the laser-cladding technique upon the microstructure and the corrosion resistance of magnesium-based alloys. The cladding apparatus and techniques have been adapted for magnesium cladding to overcome the oxidation and high vapour pressure-related problems. Laser-clad $Mg_{27}Al_{73}$, $Mg_{53}Al_{47}$, and $Mg_{72}Al_{28}$ have been obtained. Eutectic phases were observed in the two magnesium-rich alloys and in the interface of the aluminium-rich alloy. Polycrystalline structure was formed in $Mg_{27}Al_{73}$. Laser-clad $Mg_{27}Al_{73}$ was found to be superior to laser-clad Mg–5 wt% Zr, Mg–2 wt% Zr, cast AZ91B and cast magnesium in corrosion properties.

1. Introduction

Although magnesium and its alloys have some very attractive properties such as low density and superb machinability, they have not yet found widespread application as an engineering material due to their poor environmental performance and mechanical properties. The extreme position of magnesium in the electrochemical series coupled with the fact that, unlike aluminium, magnesium is unable to form protective self-healing passivating surface films in corrosive environments, make it vulnerable to glavanic attack. When coupled with a nobler metal, magnesium undergoes anodic dissolution and hence exhibits poor corrosion resistance.

Rapid solidification processing (RSP) has been identified as a most promising approach to improve corrosion properties of magnesium alloys [1–3]. Aluminium is a well-known solid solution strengthener in magnesium and is widely used in magnesium alloys. Das and Chang [4] reported that an Mg–Al-based alloy prepared using RSP exhibited a remarkably reduced corrosion rate. RS Mg–23.4 wt % Al had a corrosion rate at least two orders of magnitude lower than the corresponding chill-cast material [5]. From an investigation of binary RS magnesium alloy ribbons, Makar and Kruger [6] found that aluminium is the only element to cause a significant decrease in corrosion rate of magnesium alloys with increasing concentration to above 28.8 wt %. Also the rare-earth alloying additions increase corrosion resistance in Mg–Al-based alloys [6, 7].

In the RSP category, laser processing is an important method by which to improve the corrosion behaviour of materials. Earlier work indicated that laser surface melting improves the intergranular corrosion of stainless steel [8]. For magnesium alloys, the corrosion rate of Mg–Zn alloy was reduced by laser-remelted RSP because of the solution of the finely distributed interdendritic nonequilibrium Mg_7Zn_3 phase [9]. The corrosion resistance of Mg–Li-based alloy was substantially increased by laser-surface treatment which caused a homogeneous fine-grained microstructure [10].

The laser cladding technique provides an unique means of synthesizing non-equilibrium alloys due to its inherent rapid solidification rate [11], which promotes the formation of either an amorphous phase or non-equilibrium crystalline phases. Proper selection of alloying elements during laser cladding provides a passivating film system, which greatly reduces the galvanic action, thereby increasing the corrosion resistance of the alloys. Under the laser-cladding category, the Mg–Zr system has already been studied and reported in an earlier publication [12]. This paper reports the laser-cladding experimental technique for Mg–Al alloys, the initial characterization of microstructure, and corrosion properties.

2. Experimental procedure

2.1. Magnesium-cladding technique

The standard laser-cladding procedure was reported in earlier publications [12–15]. Here the specific changes required in the technique for magnesium cladding are reported. To reduce oxidation, magnesium cladding is carried out in a chamber in which the shielding argon pressure is above ambient pressure. The chamber dimensions are 35 cm × 35 cm × 35 cm. The chamber remains fixed on a stationary stage during cladding. Fig. 1 depicts the translation system and the powder delivery system of the chamber. The translation system allows movement in two

0022–2461 © *1993 Chapman & Hall*

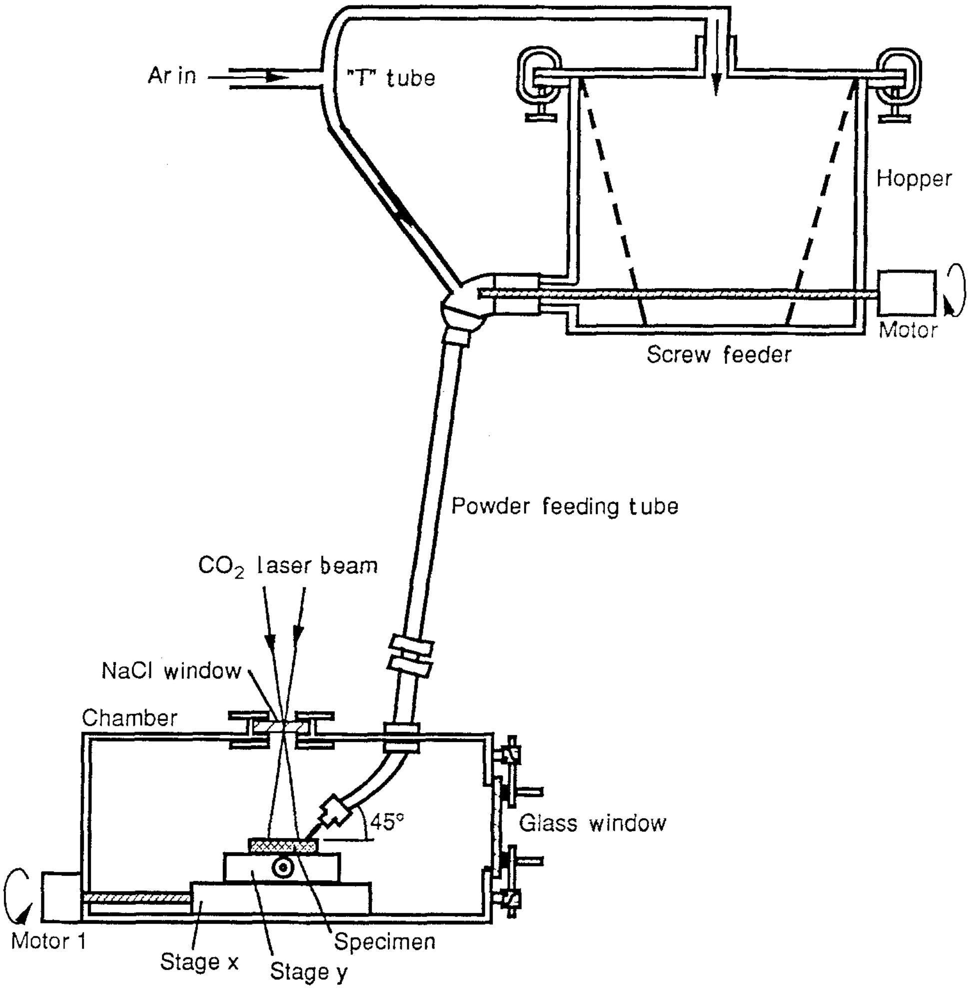

Figure 1 Schematic diagram of the powder delivery and substrate movement system.

dimensions using stages driven by stepping motors which are manipulated by a microprocessor controller, a monitor and a keyboard.

Modifications of the powder delivery gas apparatus were made for this application. If the chamber is pressurized to about 3.4 kPa (0.5 p.s.i.) above ambient pressure, a pressure gradient inside the powder feeding tube results. This back pressure restricts and can even stop the powder flow. A nozzle was designed to supply a gas jet around the powder flow tube and to eliminate the back pressure in the feeding tube. An additional problem was the pressure gradient across the screw feeder: if the gradient is positive, the powder flow stopped; if negative, the powder flow is uncontrollable. Fig. 1 shows a "T" tube joint which is used to eliminate this pressure gradient between the powder disperser and delivery tube. After a new nozzle and the "T" tube were adopted, the powder flow improved remarkably. Fig. 2 shows the powder flow during actual cladding. The design for shielding gas delivery for the protection system of the NaCl window is shown in Fig. 3. It was found that helium is superior to argon in protecting the NaCl window from the magnesium vapour during cladding. An AVCO HPL 10 kW continuous-wave CO_2 laser with a TEM_{01} mode was employed for the cladding process.

Table I indicates the nominal compositions of the three groups of binary alloys chosen for laser-cladding experiments. The powder size and purity were: − 325 mesh and 99.8% for magnesium, 20 μm and 99% for aluminium, respectively. Both atomized and ground magnesium powders (same nominal particle size) were tried for Composition B but it was found that only atomized powder was suitable for cladding. The magnesium substrate purity was 99.8%. The specimen size was about 1 cm × 4 cm × 6 cm. Before cladding, the substrate was polished with 180 grit emery paper and sand blasted.

2.2. Magnesium laser-cladding parameters

Before cladding, the positions of nozzle and substrate are adjusted in order to feed the powder directly into the interface between the laser beam and the substrate. The air remaining in the chamber is purged by flowing argon for 5 min before closing the valve. The powder delivery and laser beam are controlled simultaneously. During laser cladding, the argon gas pressure was 700 kPa (100 p.s.i.) at the tank regulator, the overall flow meter reading was 25 (relative units), the "T" tube flow meter reading was $80\,cm^3\,s^{-1}$ (10 SCFH). The helium gas protecting the NaCl window was at 140 kPa (20 p.s.i.). Table II shows the range of the cladding parameters.

2.3. Microstructural analysis

After the polishing and cleaning procedure, the cross-sections of the Mg–Al laser-clad alloy sample were

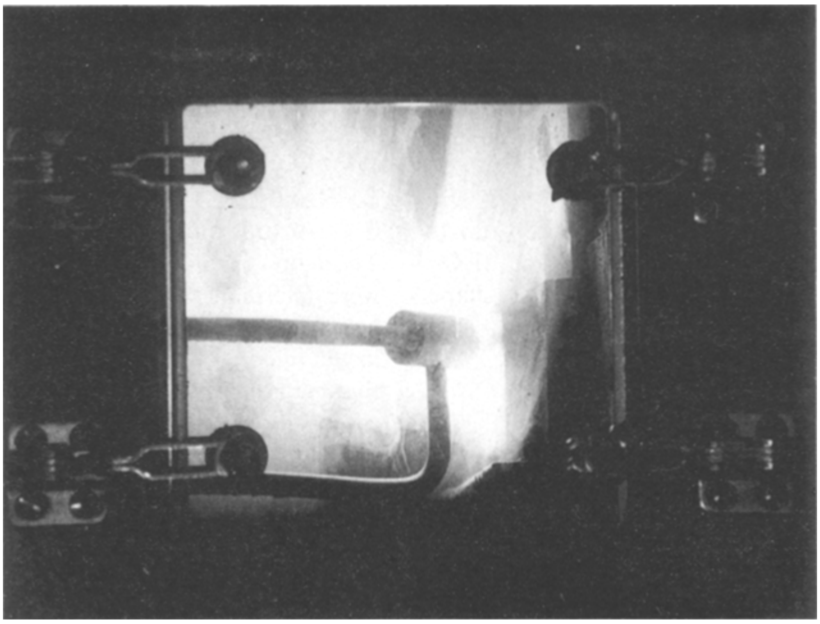

Figure 2 Photograph of the powder flow during magnesium cladding.

TABLE I Compositions of Mg–Al alloys

Alloy group	Sample number	Composition	at %		wt %	
			Mg	Al	Mg	Al
A	A1-A12	Nominal	27	73	25.0	75.0
	A6	Actual	32	68	29.33	70.22
B	B1-B4	Nominal	53	47	50.0	50.0
	B1	Actual	58	42	55.79	44.15
C	C1-C3	Nominal	72	28	70.0	30.0
	C1	Actual	80	19	77.17	20.65

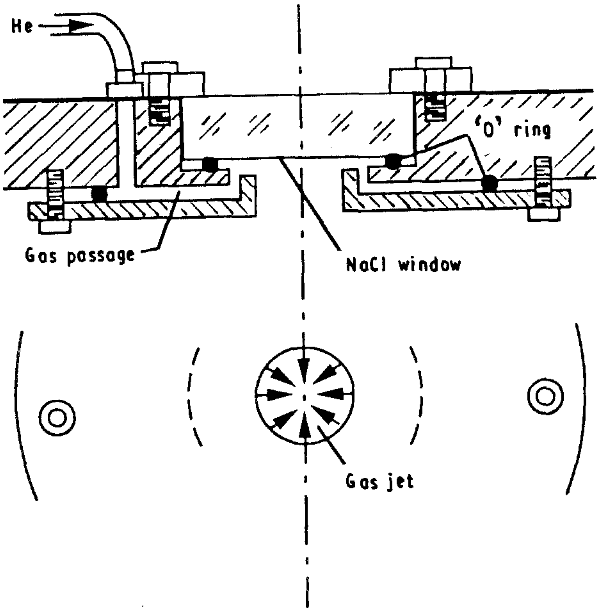

Figure 3 NaCl window protecting gas-flow passage design.

TABLE II Processing parameters

Laser power	2.0–2.8 kW
Beam diameter	3 mm
$f/\#$ of the focusing optics	cassegrain optics $f7$
Traverse speed	3.0–5.0 mm s^{-1}
Powder feed rate	0.1–0.4 g s^{-1}
Sample surface position	14 mm below focal point
Two-dimension cladding overlap coefficient	50%

observed in an optical microscope and in a Hitachi S-800 scanning electron microscope (SEM) including energy dispersive X-ray analysis (EDAX). The etchant was 6 parts HNO_3, 1 part HCl, 1 part HF, and 1 part water. The specimen was swabbed with a dilute solution of the etchant. After a reaction time of about 1 s, the samples were rinsed with tap water, cleaned with deionized water and dried. A Rigako Geigerflex X-ray diffractor was used to investigate the cladment of three alloys. For Sample A5 of $Mg_{27}Al_{73}$, a Philips 400 transmission electron microscope (TEM) was also employed to observe the crystal structure. Twin-jet electro-chemical polishing was utilized for specimen preparation. The conditions used for jet polishing were: Electrolyte, 20% perchloric acid, 80% ethanol; condition, 50 V, 60 mA, $-30\,^{\circ}$C.

2.4. Differential thermal analysis (DTA)

DTA was performed with a Perkin-Elmer system 4/7. The reference sample was Al_2O_3, the heating rate was 20 °C min^{-1}, and the scanning range was 50–700 °C under an argon flow of 40 ml min^{-1}. Before the test, the sample was cleaned with acetone, then ultrasonically cleaned in deionized water for 5 min. The sample was weighed before and after each DTA run. It was observed that the sample lost weight, the Al_2O_3 powder colour turned to black, and the sample shape did not change after the DTA run.

2.5. Corrosion tests

The corrosion behaviour of laser clad $Mg_{27}Al_{73}$ was evaluated by using a EG and F Parc Model 351 corrosion measurement system. The cleaning procedure and operation sequence could remarkably influence the results of corrosion tests. A fresh surface was obtained by abrading the sample on 320–600 grit silicon carbide paper, rinsing in deionized water and ultrasonic cleaning for 5 min in acetone. If necessary, the samples were cleaned with acetone or methanol again. After the corrosion cell was set up, the 3.5% NaCl electrolyte was added to the cell. The test was started as soon as the whole surface of the sample was immersed. For the sake of comparison, corrosion tests were also performed for magnesium and AZ91B samples. To allow comparison of different materials, every test was run using the same procedure and the same parameters.

The corrosion measurement regimen includes the following tests.

1. Corrosion potential (E_{corr}): the potential at the surface of the specimen is measured with reference to a standard calomel electrode as a function of time. The experiment indicates the rate at which E_{corr}, the equilibrium corrosion potential obtained from the horizontal portion of the curve displayed is achieved. The open circuit potential was recorded. Run time was 1800 s without initial delay.

2. Potentiodynamic anodic polarization: the specimen current was monitored when the sample was driven from $E_{corr} - 250$ mV to 0.6 V with a scanning rate of 0.4 mV s^{-1}, and the initial delay was 3600 s. The resulting curve of this applied voltage versus the logarithm of the current density is utilized to assess the corrosion resistance of the sample material.

3. Tafel plot: in this test, a controlled-potential scan is applied to a specimen from $E_{corr} - 250$ mV to $E_{corr} + 250$ mV. The scanning rate was 1 mV s^{-1} and the initial delay was 3600 s. The logarithm of the current value as a function of voltage was monitored. The slope of this Tafel plot in the linear region in the anodic direction is referred to as the anodic Tafel constant, while the cathodic constant can be obtained in the cathodic direction. Values of the corrosion current, i_{corr}, given in this report were found from the intersection of these two linear plots.

4. Polarization resistance: this test was carried out by applying a controlled-potential scan over a small range, from $E_{corr} - 20$ mV to $E_{corr} + 20$ mV. The scanning rate was 1 mV s^{-1} for $Mg_{27}Al_{73}$ and magnesium and 0.1 mV s^{-1} for AZ91B. The initial delay was 3600 s. The resulting current was linearly plotted against potential. The slope of this curve at E_{corr} is referred to as the polarization resistance.

3. Results

3.1. Actual compositions

The actual chemical compositions after laser cladding were determined by Galbraith Laboratories, Inc. The laser-cladding parameters of the analysis samples are in the middle of the parameter range. Table I shows that magnesium is about 5%–8% higher in the actual compositions than in the nominal compositions, which indicates that magnesium dilution from substrate to cladment was serious. This effect indicates that the composition of the powder must be adjusted accordingly to achieve the desired composition.

3.2. Preliminary identification of the microstructure

From SEM analysis, a magnesium-rich eutectic phase and α-magnesium or α-aluminium and β phases were obtained in laser-clad Mg–Al alloys. In $Mg_{53}Al_{47}$ and $Mg_{72}Al_{28}$, fine eutectic and α-magnesium structures were mainly observed. Fig. 4a and b taken from Sample C1 ($Mg_{72}Al_{28}$) show the eutectic and α-magnesium (dark flower-shaped region) phases. Sample B1 ($Mg_{53}Al_{47}$) has a microstructure similar to Sample C1. Fig. 5 is the equilibrium Al–Mg phase diagram [16] which does predict some of the phases. In the cladding of $Mg_{53}Al_{47}$, the α-magnesium phase is surrounded by eutectic near the interface while a large continuous eutectic area is present in the middle. There is another magnesium-rich phase formed in both B1 and C1 (see Fig. 4c, Region A). In $Mg_{27}Al_{73}$, a magnesium-rich eutectic phase was obtained at the interface. In Fig. 6a of Sample A4, the eutectic spacing was about 20–30 μm. In the bulk of the cladment, α-aluminium was formed (see Fig. 6b, the bright flower-shaped region) and surrounded by the second phase which was identified as β. The estimation of volume fraction of phases is shown in Table III.

X-ray diffraction results are shown in Fig. 7. From Fig. 7a, it is identified that the second phase in $Mg_{27}Al_{73}$ is β, Mg_2Al_3 [17]. For magnesium-rich alloys, the equilibrium phase diagram predicts that the magnesium-rich eutectic is formed from α-magnesium and γ. Fig. 7b displays the diffraction peaks for α-magnesium and γ which agree with above predictions and suggests that another magnesium-rich phase in $Mg_{72}Al_{28}$ is γ, $Mg_{17}Al_{12}$ [17]. The intensity of γ peaks is much higher in $Mg_{53}Al_{47}$ than in $Mg_{72}Al_{28}$, while the intensity of magnesium peaks is much lower in $Mg_{53}Al_{47}$.

The influence of the laser-processing parameters upon the microstructure $Mg_{27}Al_{73}$ was investigated. Table IV shows the parameters for different samples. The specific energy for A4 was double that for A3 and A2 for a given pass. But A3 was double passed while A2 was single passed. The higher specific energy for A4 is associated with the thickest eutectic interface

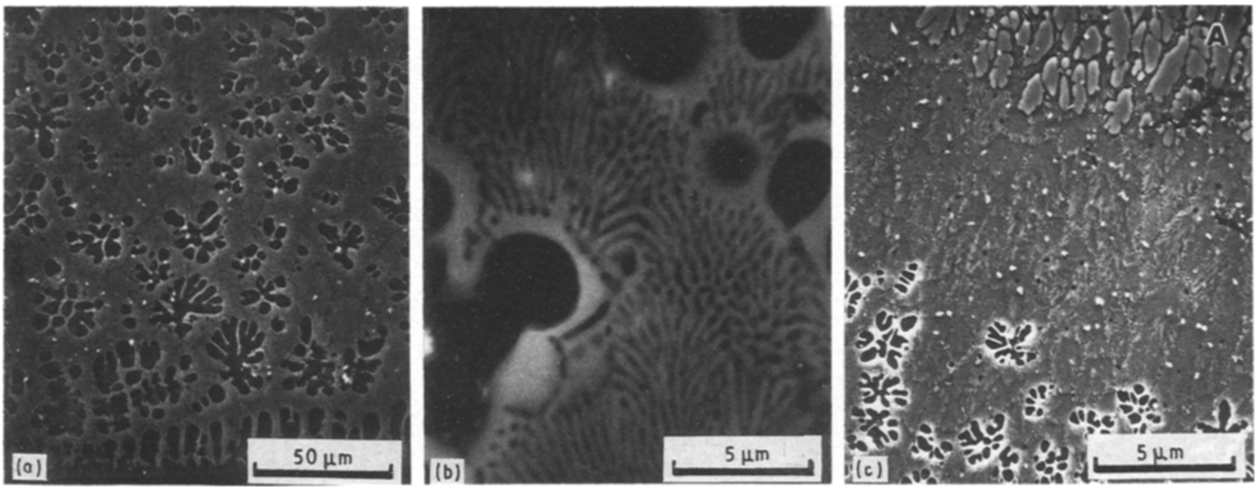

Figure 4 Scanning electron micrographs of Sample C1 ($Mg_{72}Al_{28}$): (a) the α-magnesium phase surrounded by the eutectic phase in the region near interface; (b) same field as (a) at higher magnification; (c) taken from the bulk of the cladment. Region A is γ.

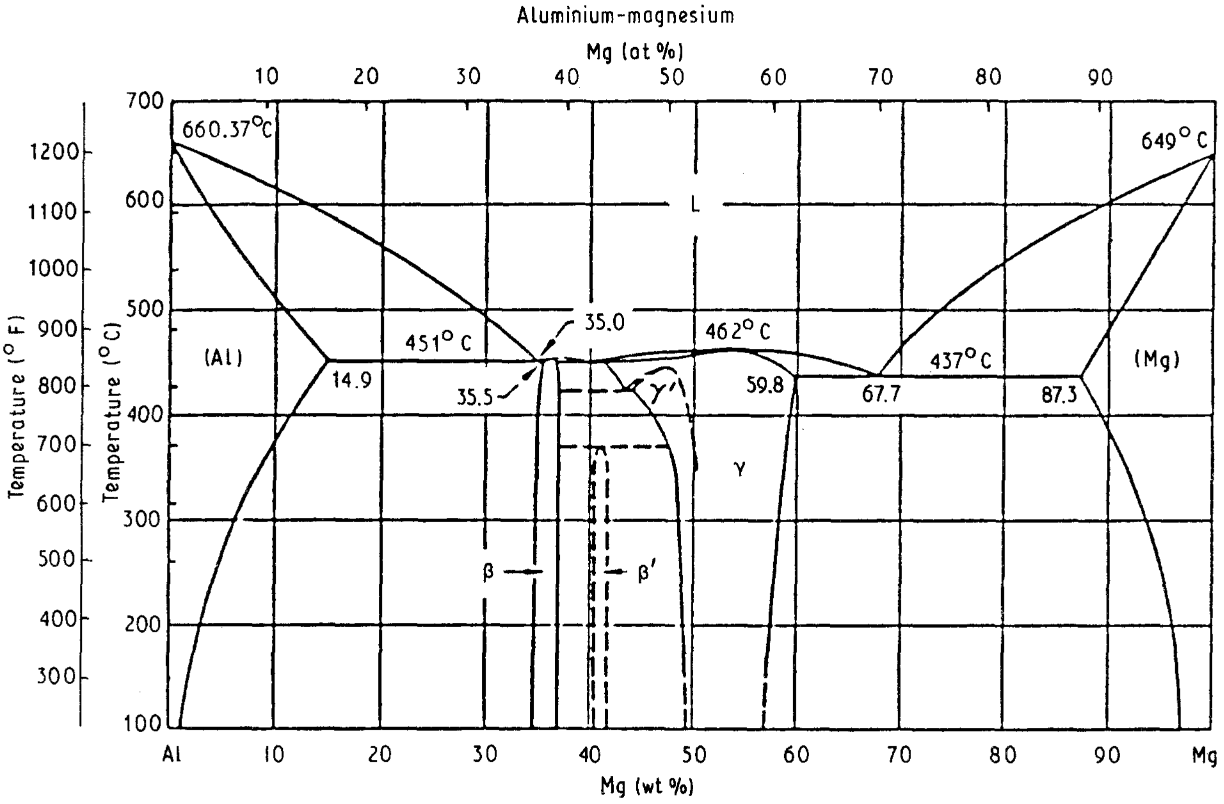

Figure 5 Al–Mg equilibrium phase diagram [16].

(20–30 µm) as shown in Fig. 6a. From Fig. 6b and c it is found that the α-aluminium area was smallest in A4 and largest in A2 while the β phase area was largest in A4 and smallest in A2. In the case of the lowest laser powers and medium specific energy for Sample A1, poor bonding between the cladment and substrate was formed.

However, TEM analysis is very limited in the current work because of the difficulties in preparation of specimen foil. The initial results for Specimen A5 of $Mg_{27}Al_{73}$ are shown in Fig. 8. In Fig. 8a, there is a series of diffraction ring patterns taken from α-aluminium indexed as from plane (1 1 0) of fcc, which suggests that there is a randomly oriented polycrystalline structure of α-aluminium. Fig. 8b shows the polycrystal diffraction rings superimposed on the spot pattern. On the other hand, β, Mg_2Al_3, is known as a partially disordered fcc structure [18]. The lattice parameters are $a = 0.40494$ nm for aluminium, $a = 2.8239$ nm for Mg_2Al_3 [17].

3.3. Differential thermal analysis (DTA) results

Fig. 9a–f show the DTA results. The phase transformation temperatures were determined by DTA survey for all three alloys. It was found that when the laser-cladding parameters were in the ranges of laser

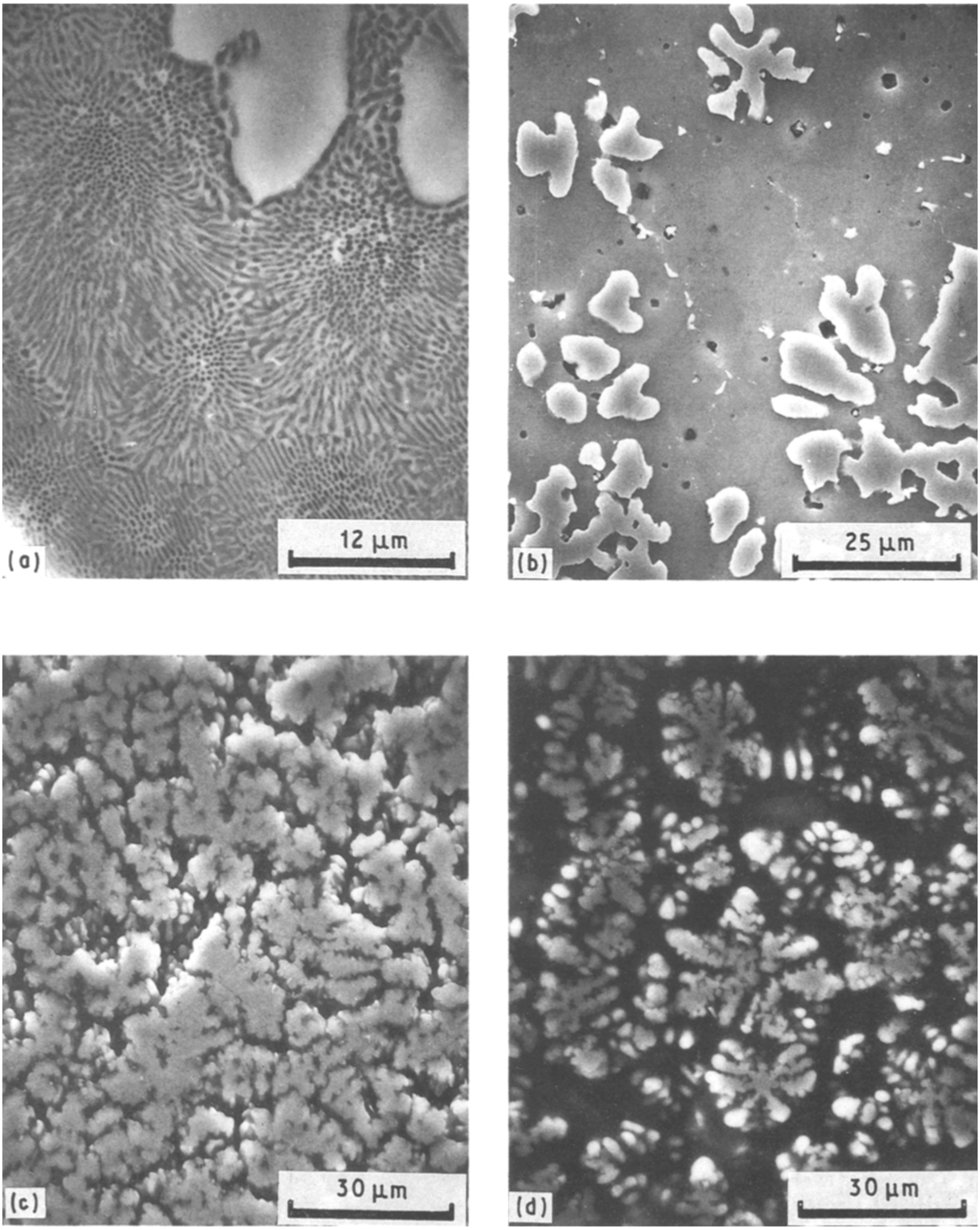

Figure 6 Scanning electron micrographs for $Mg_{27}Al_{73}$: (a) the eutectic phase in the clad-substrate interface taken from Sample A4; (b) the α-aluminium phase surrounded by the β phase in the bulk of the cladment in A4; (c) the α-aluminium phase and β phase taken from Sample A2; (d) the α-aluminium phase and β phase taken from Sample A3.

power 2.0–2.4 kW, beam diameter 3 mm and traverse speed 3–5 mm s^{-1}, a eutectic dissolution endothermic peak began at about 437 °C for Sample B1 of $Mg_{53}Al_{47}$ and Sample C1 of $Mg_{72}Al_{28}$ (see Fig. 9a and b), and α-magnesium dissolution ended at 510 °C for B1, 550 °C for C1. In the same range of laser-cladding parameters, it was also found that a β phase transformation endothermic peak began at about 447 °C for $Mg_{27}Al_{73}$ (see Fig. 9d–f). For $Mg_{27}Al_{73}$

TABLE III Phase volume fraction

Sample	Nominal composition	Phase volume fractions		
A4	$Mg_{27}Al_{73}$	α-Al 30%	β 70%	
B1	$Mg_{53}Al_{47}$	α-Mg 15%	Eut. 78%	Other 7%
C1	$Mg_{72}Al_{28}$	α-Mg 39%	Eut. 56%	Other 5%

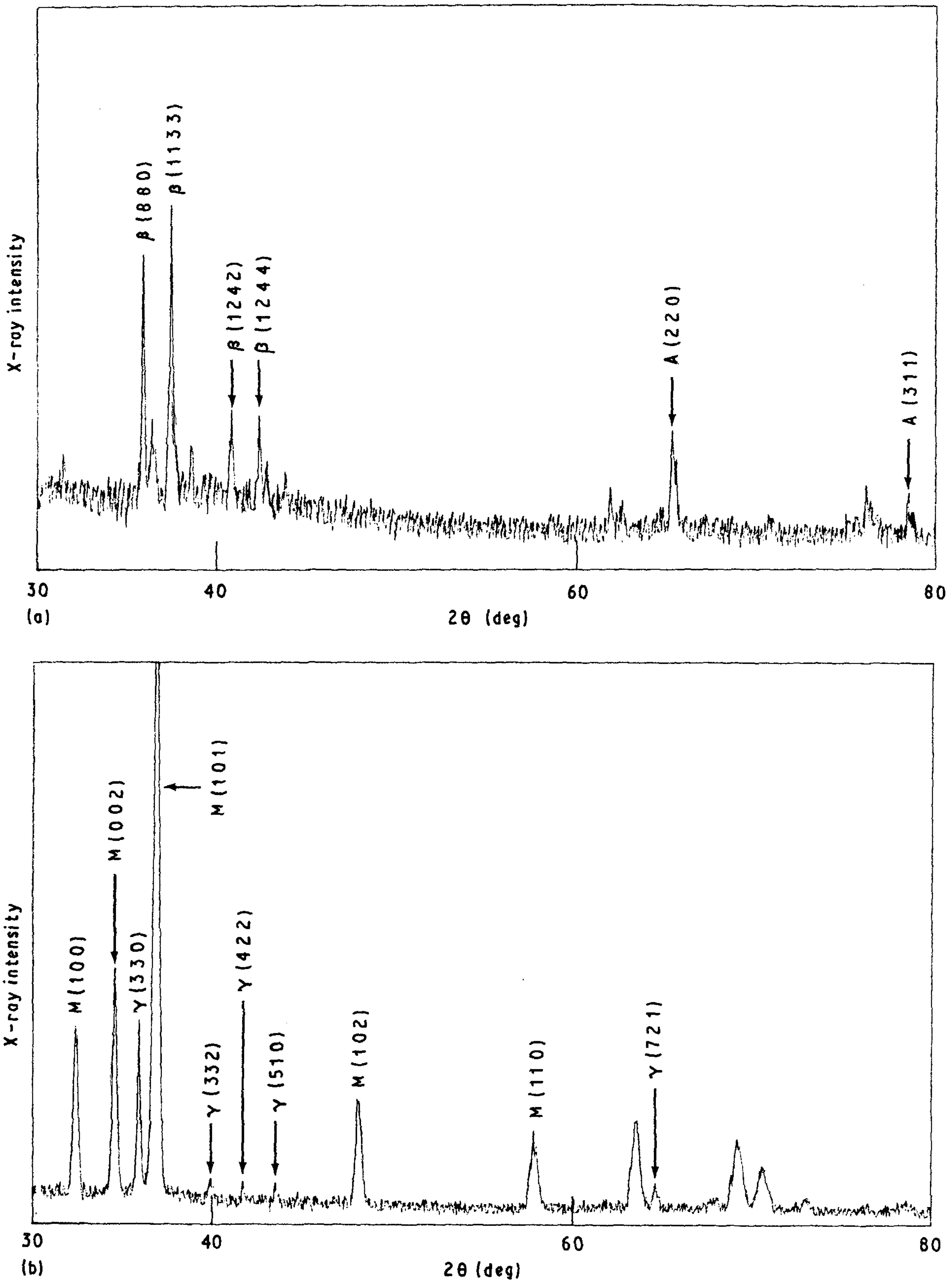

Figure 7 X-ray diffraction results for Samples (a) A4 of $Mg_{27}Al_{73}$, (b) C1 of $Mg_{72}Al_{28}$. A = aluminium, β = Mg_2Al_3, M = magnesium, γ = $Mg_{17}Al_{12}$.

alloys, the eutectic region in the DTA sample was almost completely removed during polishing, therefore, the phase transformation endothermic peak came from the β and α-aluminium phases.

The DTA results for $Mg_{27}Al_{73}$ clad with different values of processing parameters (see Table IV) indicate the influence of laser-cladding techniques upon the same microstructure. In the Fig. 9c, for Sample A1 (laser power 1.5 kW, specific energy 200 J mm^{-2}), there is only a big α-aluminium dissolution peak which implies on β phase in this sample. In Fig. 9d, for Sample A2 (2.4 kW, 160 J mm^{-2}), there is a small β

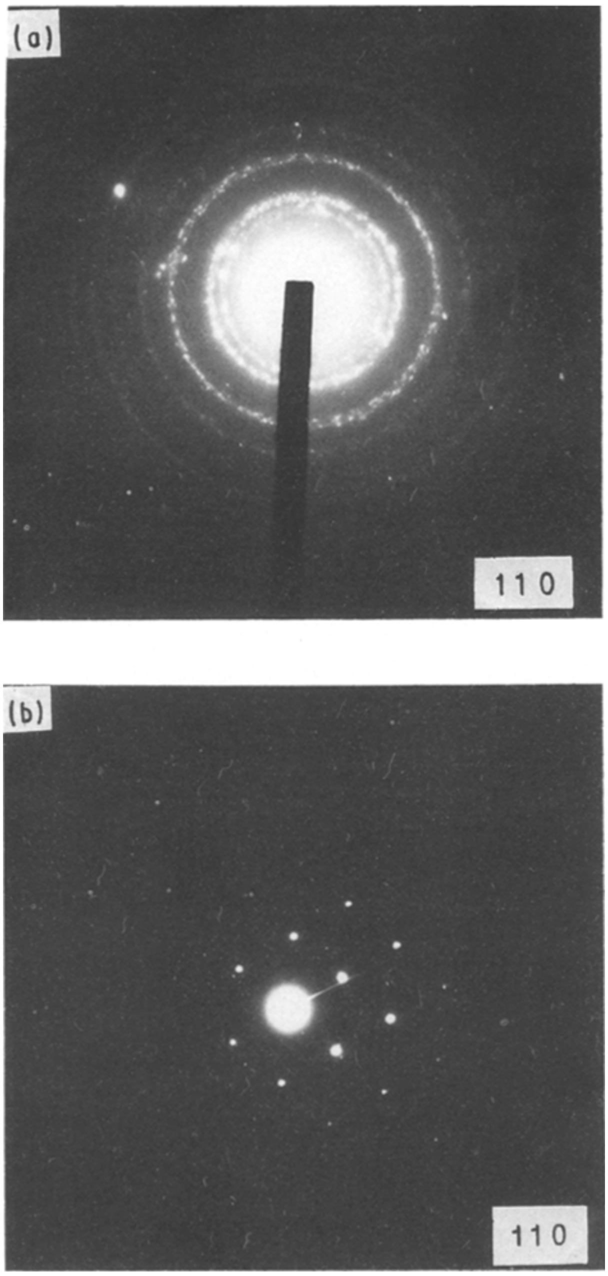

Figure 8 Electron diffraction pattern obtained by TEM taken from α-aluminium phase in A5 of $Mg_{27}Al_{73}$: (a) polycrystal diffraction rings from plane (1 1 0) of fcc; (b) polycrystal diffraction pattern superimposed on the spot pattern from plane (1 1 0) of fcc.

dissolution peak and a big α-aluminium dissolution peak, associated with the different phase concentrations. Fig. 9e, for Sample A3 (2.4 kW, 160 J mm^{-2}, double pass), implies an increase in β phase concentration caused by the use of a double laser pass. In the case of Sample A4 (2.4 kW, 320 J mm^{-2}), there is a much deeper β dissolution peak, associated with the highest specific energy. All the above results agree well with the microstructures shown in Fig. 6, indicating that the phase concentration can be controlled by varying the laser-cladding parameters. It is clear that not only specific energy but also laser power influence the microstructure.

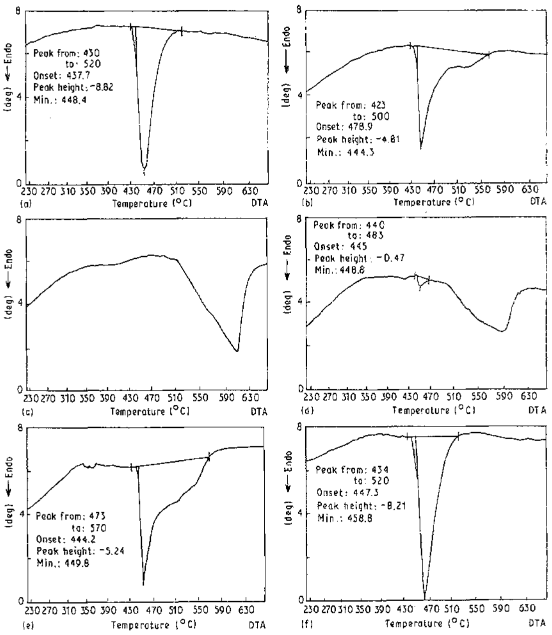

Figure 9 DTA results for Samples (a) B1 of $Mg_{53}Al_{47}$, (b) C1 of $Mg_{72}Al_{28}$, (c) A1, (d) A2, (e) A3, (f) A4 of $Mg_{27}Al_{73}$. Weights: (a, b) 34.80 mg, (c) 72.00 mg, (d, e) 70.10 mg, (f) 54.90 mg. Scan rate 20 °C min^{-1}, argon atmosphere, 4 ml min^{-1}.

TABLE IV Parameters for $Mg_{27}Al_{73}$ samples

	Sample			
	A1	A2	A3	A4
Laser power (kW)	1.5	2.4	2.4	2.4
Beam diameter (mm)	3.0	3.0	3.0	3.0
Traverse speed (mm s^{-1})	2.5	5.0	5.0	2.5
Number of passes	1	1	2	1
Specific energy (J mm^{-2})	200	160	160	320
Micrograph figure	–	6c	6d	6b
DTA figure	9c	9d	9e	9f

[a] For different tests, the specimens with same cladding parameters have the same number.

3.4. Corrosion test results for $Mg_{27}Al_{73}$

From the corrosion tests for laser-cladding alloy $Mg_{27}Al_{73}$, commercially produced alloy AZ91B and pure magnesium in 3.5 wt % NaCl electrolyte, the results presented in Tables V–VII and Fig. 10 were obtained. The corrosion potential data of laser-clad Mg–2 wt % Zr and Mg–5 wt % Zr [12] in 3.5% NaCl were also adopted in Table V for comparison.

These results indicate that laser-clad $Mg_{27}Al_{73}$ is superior to laser-clad Mg–2 wt % Zr, Mg–5 wt % Zr, AZ91B and magnesium in corrosion properties. The corrosion rate (CP) of $Mg_{27}Al_{73}$ in one order of magnitude lower than that of AZ91B and two orders of magnitude lower than that of magnesium. In potentiodynamic tests, the clad materials passivated spontaneously during the 3600 s initial delay, while magnesium and AZ91B have no potential region over which the sample surface remained passive. Fig. 10a shows that the $Mg_{27}Al_{73}$ sample remained passive over a potential region of 200 mV where the current was quite stable. The passive film began breaking at about − 1.0 V potential. In the case of AZ91B, when the applied potential was above − 1.6 V, the passive

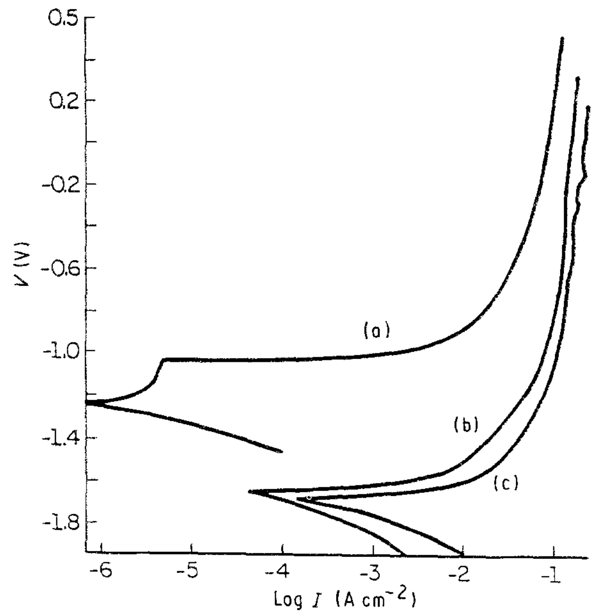

Figure 10 Corrosion results of potentiodynamic anodic polarization for alloys (a) laser-clad $Mg_{27}Al_{73}$, (b) cast AZ91B, (c) cast magnesium.

film broke as indicated by the current increasing rapidly with a slight increase in potential (see Fig. 10b). The passive film was broken completely when the potential was about − 1.4 V. Similar results were found for magnesium (see Fig. 10c). These effects indicate that the passive film on $Mg_{27}Al_{73}$ is much more stable than the passive film on AZ91B. In Table VII, the slope ($\Delta V/\Delta I$) at E_{corr} for $Mg_{27}Al_{73}$ is much larger than the corresponding slopes for AZ91B and magnesium, which again indicates that the laser-clad alloy $Mg_{27}Al_{73}$ is more corrosion resistant than case AZ91B and cast pure magnesium in 3.5% NaCl solution.

TABLE V Corrosion potential, E_{corr}

Alloy	E_{corr} in 3.5 wt % NaCl with reference to SCE[a] (V)
Mg-75 wt % Al($Mg_{27}Al_{73}$)	− 1.06
Mg-5 wt % Zr	− 1.57
Mg-2 wt % Zr	− 1.61
AZ91B	− 1.65
Mg	− 1.73

[a] SCE: standard calomel electrode.

TABLE VI Corrosion current i_{corr}, and corrosion rate, CR

Alloy	i_{corr}(μA cm^{-2})	(CR 10^{-3} in/year)
$Mg_{27}Al_{73}$	3.16	4.5
AZ91B	31.6	29.2
Mg	500.0	453.9

TABLE VII Polarization resistance, $\Delta V/\Delta I$ at E_{corr}

Alloy	Polarization resistance (%)
$Mg_{27}Al_{73}$	145 000
AZ91B	42500
Mg	12.5

* All the above were obtained in 3.5 wt % NaCl electrolyte.

4. Discussion

In the current work, three Mg–Al laser-clad alloys have been obtained. The oxidation problem has been overcome to a large extent with the adaptation of the shielding gas chamber, the powder feeding nozzle, and the gas delivery system. Generally, the $Mg_{27}Al_{73}$ clad has less porosity than other alloys. For magnesium-rich laser-clad alloys the cladments are still thin because of the low molten cladment surface tension and high evaporation losses.

The results show that magnesium alloys rich in eutectic phase can be obtained for magnesium-rich compositions by laser cladding. Because the phase concentration can be controlled by the laser-cladding parameter, if we choose a composition around 60–70 wt % Mg (see Fig. 5) and optimize parameters, 100% eutectic structure could be obtained. The alloys with around 45–55 wt % Mg might be multiphase structured, according to the equilibrium phase diagram and the investigation for $Mg_{53}Al_{47}$ which was found to be very brittle during sample preparation.

For $Mg_{27}Al_{73}$ alloy, α-aluminium and β phases are formed instead of α-aluminium and eutectic as predicted by the equilibrium phase diagram. This effect implies that eutectic formation was totally suppressed by the rapid quenching inherent in laser cladding. The influence of laser-cladding parameter upon microstructure suggests that a single phase of β, Mg_2Al_3, could possibly be obtained in composition around 30–35 wt % Mg.

It is believed that the partially disordered structure in β which looks quite homogeneous at magnifications of × 1200–3500, and randomly oriented aggregate polycrystal structures in α-Al are the dominant source of the superior corrosion properties of $Mg_{27}Al_{73}$. From the lamellar spacing of eutectic in the interface of Sample A4 (see Fig. 6a), a cooling rate of 10^4–10^5 K s^{-1} is estimated [19]. In future work, if the cooling rate could be increased sufficiently, an amorphous phase structure will be expected in single phase, β alloy or in β and α-aluminium structure alloy with high corrosion resistance properties.

The results and understanding are preliminary and limited by the accuracy of the analysis. The conditions for the electrochemical polishing of samples must be found for the TEM analysis which will supply more information to understanding the non-equilibrium processing including solute solubility extension and the existence of metastable phases.

5. Conclusions

Both magnesium- and aluminium-rich magnesium alloys were prepared using a laser-cladding technique.

A magnesium-rich eutectic phase and the α-magnesium phase were obtained in magnesium-rich alloys ($Mg_{53}Al_{47}$ and $Mg_{72}Al_{28}$). A β phase and α-aluminium phase were obtained in the bulk of the cladment of aluminium-rich alloys ($Mg_{27}Al_{73}$) while a eutectic phase was also formed at the interface of this alloy. The polycrystalline structure was formed in $Mg_{27}Al_{73}$. The eutectic concentration in magnesium-rich alloys and the β phase concentration in aluminium-rich alloys can be controlled by varying the laser-cladding parameters. The corrosion resistance of laser-clad alloy $M_{27}Al_{73}$ is superior to that of laser-clad Mg–2 wt % Zr, Mg–5 wt % Zr, cast AZ91B and magnesium.

Acknowledgements

This work was sponsored by the Air Force Office of Scientific Research under the contract no. AFOSR-89-0061. Dr Alan Rosenstein was the program manager. The electron microscopy analysis was performed at the Center for Microanalysis of Materials, operated by the Materials Research Laboratory, University of Illinois at Urbana-Champaign (UIUC). We also thank Mr Justin Koch, Materials Engineering Research Laboratory (UIUC), for the help during magnesium cladding experiments.

References

1. A. JOSHI and R. E. LEWIS, "Literature Review and Interim Technical Report-Rapid Solidified Magnesium Alloys", AFWAL Contract F33615-85-C-5032, Lockheed Missiles and Space Company, Inc., Report no. LMSC–F083181, January 1986.
2. R. E. LEWIS and A. JOSHI, in "Processing of Structural Metals by Rapid Solidification", edited by F. H. Froes and S. J. Savage (American Society for Metals, Metals Park, pp. 367–78.
3. A. JOSHI and R. E. LEWIS, in "Advances in Magnesium Alloys and Composites", edited by H. Paris and W. H. Hunt (The Minerals, Metals and Materials Society, 1988) pp. 89–103.
4. S. K. DAS and C. F. CHANG, in "Rapidly Solidified Crystalline Alloys", edited by S. K. Das, B. H. Kear and C. M. Adam (Metal Society, Warrendale, PA, 1985) pp. 137–56.
5. F. HEHMANN, R. G. J. EDYVEAN, H. JONES and F. SOMMER, in "International Conference on (PM) Aerospace Materials", Metal Powder Report, Luzern, Switzerland, 2–4 November 1987 (MPR Publishing, Shrewbury, 1988) pp. 46.1–46.16.
6. G. L. MAKER and J. KRUGER, in "Advances in Magnesium Alloys and Composites", edited by H. Paris and W. H. Hunt (The Minerals, Metals, and Materials Society, Warrendale, PA, 1988) pp. 105–21, 1988.
7. C. F. CHANG, S. K. DAS and D. RAYBOULD, in "Rapidly Solidified Materials", edited by P. W. Lee and R. S. Carbonara (American Society for Metals, Metals Park, 1986) pp. 129–35.
8. T. R. ANTHONY and H. E. CLINE, *SPIE, Laser Applic. Mater. Process.* **198** (1979) 82.
9. T. Z. KATTAMIS, in "Laser in Metallurgy", edited by K. Mukherjee and L. Mazumder (Metallurgical Society of AIME, Warrendale, PA, 1981) pp. 1–10.
10. R. Kh. KALIMULLIN and Yu. Ya. KOZHEVNIKOV, in "Metal Science and Heat Treatment", Vol. 27 (3–4) (Plenum, NY, 1985) pp. 272–4, translated from Russian.
11. J. MAZUMDER, S. SIRCAR, C. RIBANDO and A. KAR, *J. Laser Applic.* March **1** (1989) 27.
12. R. SUBRAMANIAN, S. SIRCAR and J. MAZUMDER, *J. Mater. Sci.* **26** (1991) 951.
13. V. M. WEERASINGHE and W. M. STEEN, in "Proceedings of The 4th International Conference on Laser Processing", Los Angeles, January 1983, E. Metzbower (ed), (American Society of Metals, OH) pp. 166–74.
14. L. J. LI and J. MAZUMDER, in "Laser Processing of Materials", edited by K. Mukherjee and J. Mazumder (Metal Society of AIME, Warrendale, PA, 1985) pp. 35–50.
15. S. SIRCAR, J. SINGH and J. MAZUMDER, *Acta Metall.* **37** (1989) 1167.
16. T. LYMAN (ed) "Metals Handbook" 28th edn. Vol. 8 (American Society for Metals, OH 1973) p. 261.
17. "JCPDS Powder Diffraction File Inorganic Phases" card 3-877, 1-1128, 28-48, 34-1035 (International Center for Diffraction Data 1989).
18. S. SAMSON, *Acta. Crystallogr.* **19** (1965) 401.
19. R. TRIVEDI and W. KURZ, "Solidification Processing of Eutectic Alloys" (The Metallurgical Society, Warrendale, PA, 1988) pp. 3–34.

Received 6 July
and accepted 10 October 1990